journal

J. Am. Ceram. Soc., 99 [3] 1031–1041 (2016)
DOI: 10.1111/jace.13971

Factors Influencing the Stability of AFm and AFt in the Ca–Al–S–O–H System at 25°C

Pan Feng,[‡,§,†] Changwen Miao,[‡,¶] and Jeffrey W. Bullard[§]

[‡]Jiangsu Key Laboratory of Construction Materials, School of Material Science and Engineering, Southeast University, Nanjing 211189, China

[§]Materials and Structural Systems Division, National Institute of Standards and Technology, Gaithersburg, Maryland

[¶]Jiangsu Research Institute of Building Science Co., Ltd, Nanjing, Jiangsu 210008, China

The stabilities of Al_2O_3–Fe_2O_3-mono (AFm) and -tri (AFt) phases in the Ca–Al–S–O–H system at 25°C are examined using Gibbs energy minimization as implemented by GEM-Selektor software coupled with the Nagra/PSI thermodynamic database. Equilibrium phase diagrams are constructed and compared to those reported in previous studies. The sensitivity of the calculations to the assumed solid solubility products, highlighted by the example of hydrogarnet, is likely the reason that some studies, including this one, predict a stable SO_4-rich AFm phase while others do not. The majority of the effort is given for calculating the influences on AFm and AFt stability of alkali and carbonate components, both of which are typically present in cementitious binders. Higher alkali content shifts the equilibria of both AFt and AFm to lower Ca but higher Al and S concentrations in solution. More importantly, higher alkali content significantly expands the range of solution compositions in equilibrium with AFm. The introduction of carbonates alters not only the stable AFm solid solution compositions, as expected, but also influences the range of solution pH over which SO_4-rich and OH-rich AFm phases are dominant. Some experimental tests are suggested that could provide validation of these calculations, which are all the more important because of the implications for resistance of portland cement binders to external sulfate attack.

I. Introduction

Al2O_3–Fe_2O_3-mono and -tri phases (AFm and AFt, respectively), both of which are among the hydration products of ordinary portland cement binders, have significant impact on setting,[1] early-age strength gain,[2] and longer term performance properties such as external sulfate resistance[3–5] and ability to bind radionuclides.[6] This importance has led to the publication of experimental and theoretical investigations of the stability of these phases, which is a central factor governing their abundance in cementitious binders.

The literature on stability of AFm phases is complicated by the wide range of compositions and structural variants, and by the evident sensitivity of measurements to phase synthesis procedures and laboratory conditions.[7–17] Just to take the example of calcium monosulfoaluminate, an AFm phase saturated with respect to sulfate anions, and hereafter called simply monosulfate, Damidot et al.[11–13] calculated that it is metastable with respect to a mixture of hydrogarnet and ettringite at temperatures below 50°C. In contrast, Albert et al.[15] reported that monosulfate is stabilized if the activity of water is less than unity, which it is for any solution other than pure water. More recently, using higher values of hydrogarnet's solubility product, Matschei et al.[16] calculated monosulfate to be stable at temperatures above 5°C.

Glasser[14] has shown that experimentally determining the thermodynamic stability conditions in aqueous calcium sulfoaluminate systems is problematic because of (1) difficulties in preventing progressive carbonation; (2) challenges in characterization of the solid phases, which often are poorly ordered and can have variable composition; and (3) the tendency toward water loss by the higher hydrates during their characterization. Thermodynamic calculations provide a way to predict equilibrium states and relative phase stability in these multicomponent systems, and the power of this line of inquiry for cementitious system has been aided tremendously both by meticulous experimental measurement of thermodynamic properties[16–19] and by improvements in numerical methods.[20,21]

Several computer software packages are available for calculating thermodynamic equilibrium states in multicomponent systems. All of them are based on one of two approaches. The great majority of them use the solution of the coupled nonlinear equations directly minimizing the mass balance residuals, derived from the law of mass action (LMA). Software packages based on LMA include WATEQ,[22] MINEQL,[23] PHREEQC,[24] PHRQPITZ,[25] and CHESS.[26] Less common, but more general, are models based on the principle of direct Gibbs energy minimization (GEM) subject to mathematical constraints on the total composition, temperature, and hydrostatic pressure,[19,21,27–29] which simultaneously enforce the mass balance. Software packages that use the latter approach include GEM-Selektor[21] and the OLI[a,b] AQ model.[30]

LMA approaches have been used in several studies of the Ca–Al–S–O–H system.[12,15,31] But LMA algorithms typically have limited ability to solve problems involving partitioning among multiple phases that each may have variable composition because such algorithms usually must assume fixed compositions of all phases other than the aqueous solution. Lippmann diagrams[32] can be used to estimate activities or mole fractions of binary solid solution end-members in equilibrium with the aqueous solution,[33] and unified theory of solid solution solubilities can also be used for multicomponent solid mixtures,[34] but LMA methods become complicated and

R. Riman—contributing editor

Manuscript No. 36587. Received March 17, 2015; approved September 11, 2015.
[†]Author to whom correspondence should be addressed. e-mail: panda0325@163.com

[a]OLI Systems, Inc., Cedar Knolls, NJ
[b]Certain commercial software is identified in this article to foster understanding. Such identification does not imply recommendation or endorsement by the National Institute of Standards and Technology, nor does it imply that the software identified is necessarily the best available for the purpose.

inefficient for nonideal solid solutions because the equilibrium mole fractions and activity coefficients of the end-members must be known in advance. Moreover, this limitation is especially relevant to cementitious systems because several of the possible solid phases, including AFt and AFm, are known to have variable compositions that can be modeled as nonideal solid solutions. GEM methods, on the other hand, automatically partition the equilibrium mole fractions of each component among multiple nonideal solid solutions, and are therefore attractive for analyzing the multiple potential solid solutions that may form in the Ca–Al–S–O–H system.

In this article, GEM-Selektor software (Paul Scherrer Institut, Villigen, Switzerland),[21] using the Nagra-PSI thermodynamic database,[35] is used to study the stability of AFm and AFt phases in a simple Ca–Al–S–O–H system. The GEM calculations are compared to experimental measurements and GEM calculations in the recent literature[16,17,36] and to earlier LMA calculations by Damidot and Glasser.[12,13] Stable solid phases including gibbsite (AH_3),[c] hydrogarnet (C_3AH_6), portlandite (CH), as well as AFm and AFt solid solutions are identified and their stability ranges are mapped out in composition space. We also use GEM calculations to investigate the influence of alkali cations on the relative stability of AFt and AFm phases. Generally, the presence of either potassium or sodium shifts the position and shape of the surface in composition space over which AFt is stable in similar ways, but higher concentrations of potassium can also stabilize syngenite. A range of assumed solubility product values for hydrogarnet, reported in the literature, are used to test how they influence the predictions of the AFm phase equilibrium surface. Finally, the dependence of stable phase assemblages on pH and on the presence of $CaCO_3$ is investigated.

II. Thermodynamic Calculations

Our calculations are performed using the GEM-Selektor software,[21] which implements the GEM-IPM calculation method. The numerical approach is described elsewhere,[20,37] so only a sketch will be provided here. It is worth emphasizing that any numerical method that minimizes Gibbs energy should be able to reproduce the results of this article if the same thermodynamic property input data are used.

A GEM calculation is initiated by specifying the total moles of each chemical element, collectively designated as independent components (ICs). Dependent chemical components (DCs) are those solids and dissolved components, made from one or more ICs, which have fixed composition and known Gibbs energy of formation. Thermodynamic phases are composed of one or more DCs. Minimization of the Gibbs energy at fixed temperature, hydrostatic pressure, and IC mole numbers determines the equilibrium concentrations of DCs and their distribution in phases. The molar Gibbs energy is

$$G = \sum_k \sum_j x_{j,k}\mu_{j,k} \tag{1}$$

where $x_{j,k}$ and $\mu_{j,k}$ are the mole fraction and chemical potential, respectively, of the j-th DC in the k-th phase. In the absence of charged surface complexes, the chemical potential of a DC in a particular phase is given by

$$\mu_{j,k} = \mu_j^\circ(T,P) + \ln\gamma_{j,k}c_{j,k} \tag{2}$$

where μ_j° is the standard chemical potential of the j-th DC, which depends on temperature (T) and pressure (P), and, and $\gamma_{j,k}$ and $c_{j,k}$ are the molal activity coefficient and the molal concentration, respectively, of the DC component j in phase k.

The interior points method (IPM) calculates the equilibrium components $x_{j,k}$ and $\mu_{j,k}$ of the speciation vector and chemical potential vector. The minimization algorithm is based on satisfying the Karpov–Kuhn–Tucker conditions,[38] which are necessary and sufficient for the Gibbs energy in Eq. (1) to be a minimum.

The calculations just described require input of the standard molar Gibbs energies of each DC component and an activity model for the DC components in various condensed phases. These thermodynamic data were taken from the internally consistent Nagra/PSI thermodynamic data set.[35] Additional solids that are not included in the Nagra/PSI data set, but which nevertheless are expected to form in cementitious systems, are taken from compilations given by Lothenbach et al.[28] and Matschei et al.[16] that were developed to be consistent with the Nagra data set.

One of the significant improvements of GEM calculations that have been made since the LMA studies published earlier[12,13] is a more thorough accounting of DC solute components and their influence on the Gibbs energy. Thermodynamic data for a wide range of solute components are available in the Nagra-PSI database. Molal activity coefficients γ_i for individual aqueous species are calculated using the extended Debye–Hückel equation[35]:

$$\log_{10}\gamma_i = \frac{-Az_i^2\sqrt{I}}{1 + Ba\sqrt{I}} + bI \tag{3}$$

where A and B are (T,P)-dependent coefficients, z_i is the species charge, I is the molal ionic strength, $a = 3.72$ Å is the common Kielland ion-size parameter, and $b = 0.064$ is the common third parameter for background electrolyte at 25°C. The solution speciation reactions and equilibrium constants are provided in Table I.

(1) Solid Solutions for AFm and AFt Phases

The family of AFm phases are structurally related and have the general chemical formula $Ca_2(Al,Fe)(OH)_6{\cdot}X{\cdot}xH_2O$, where X represents a monovalent ion or half a divalent anion, most commonly sulfate or carbonate.[39] The basic structures of AFm phases have been determined and recently refined for several subtypes.[40–43] Due to the charge imbalance caused by the replacement of divalent ions in the structure by trivalent ions, anions such as hydroxide, sulfate, and carbonate enter the layers forming OH-AFm phase, SO_4–AFm phase (i.e., monosulfate), and hemi- or monocarboaluminate. Published studies differ on the existence and extent of solid solution between OH–AFm and SO_4–AFm phases. Either

Table I. Solution Components and Equilibrium Constants in the Nagra-PSI Database[34] Used in This Study

Species	$\log_{10} K_{sp}$
$Al^{3+} + H_2O \rightleftharpoons Al(OH)^{2+} + H^+$	−4.957
$Al^{3+} + 2H_2O \rightleftharpoons Al(OH)_2^+ + 2H^+$	−10.594
$Al^{3+} + 3H_2O \rightleftharpoons Al(OH)_3^0 + 3H^+$	−16.432
$Al^{3+} + 4H_2O \rightleftharpoons Al(OH)_4^- + 4H^+$	−22.879
$Al^{3+} + SO_4^{2-} \rightleftharpoons AlSO_4^+$	3.90
$Al^{3+} + 2SO_4^{2-} \rightleftharpoons Al(SO_4)_2^-$	5.90
$Ca^{2+} + H_2O \rightleftharpoons CaOH^+ + H^+$	−12.78
$Ca^{2+} + SO_4^{2-} \rightleftharpoons CaSO_4^0$	2.44
$H_2O \rightleftharpoons OH^- + H^+$	−14.00
$K^+ + H_2O \rightleftharpoons KOH^0 + H^+$	−14.46
$K^+ + SO_4^{2-} \rightleftharpoons KSO_4^-$	0.85
$Na^+ + H_2O \rightleftharpoons NaOH^0 + H^+$	−14.18
$Na^+ + SO_4^{2-} \rightleftharpoons NaSO_4^-$	0.7

[c]Conventional cement chemistry notation is often used in this article to specify the composition of solid phases, whereby C = CaO, A = Al_2O_3, H = H2O, and $\bar{S}$ = SO_3.

complete[7,8] or partial[14,44] miscibility have been reported. More recently, solid solutions of monosulfate with OH–AFm were detected experimentally as a function of SO_4/OH ratio.[17]

This study models these nonstoichiometric AFm and AFt phases as regular solid solutions with thermodynamic properties provided in the cemdata07 supplement database for cementitious phases.[16] The end-members used for each solid solution phase are shown in Table III. The composition and solubility products of all the possible phases, including AFm and AFt end-members, are listed in Table II. However, the only stable phases found within the range of global compositions we tested are hydrogarnet, gibbsite, AFm phase with end-members monosulfate and C_4AH_{13}, AFt, portlandite, gypsum, and syngenite. In almost all of the calculations, because iron is absent from the system, AFt is pure ettringite; the only exception is when carbonates are added to the system, in which case AFt is a solid solution, still consisting almost entirely of the ettringite end-member but with a small fraction of the tricarboaluminate end-member. For this reason, we will hereafter sometimes use the terms AFt and ettringite interchangeably.

III. Results and Discussion

A phase diagram representation of the Ca–Al–S–O–H system at 25°C is shown as a projection onto the Ca–Al–S composition subspace in Fig. 1.

The diagram was constructed by calculating equilibrium states for 240 different sets of elemental molar compositions $\{n_{Ca}, n_{Al}, n_S, n_O, n_H\}$, with the following constraints placed on $\{n_O\}$ and $\{n_H\}$:

$$n_O = 3n_{Al} + 6n_{Ca} + \left(\frac{1000}{18}\right) \quad (4)$$

$$n_H = 3n_{Al} + 2n_{Ca} + 2\left(\frac{1000}{18}\right) \quad (5)$$

These constraints mimic the process of adding aluminum as $Al(OH)_3$, sulfur as $CaSO_4$, and any additional calcium as $Ca(OH)_2$ to 1 kg of water.

When line segments are interpolated between pairs of points, a 3D figure is formed that rests on the Ca–Al plane. The Ca–Al–S–O–H system has five components, so Gibbs' phase rule indicates that up to seven phases can coexist at equilibrium in this system. Ordinarily, points in composition space where the maximum possible number of phases (n) are in mutual equilibrium are called "invariant points" because the composition cannot be varied in any way without destroying that equilibrium among those n phases. When the entire composition space can be visualized, invariant points correspond geometrically to vertices at the intersection of one-dimensional curves. Similarly, $n-1$ phases coexist along one-dimensional boundaries, $n-2$ phases coexist at 2D surfaces, and so on. However, when more than three components are present, phase diagrams generally must be rendered as projections of the composition space onto a 2D or 3D subspace. This projection necessarily breaks the geometrical correspondence just described. Thus, in Fig. 1, for example, the boundary curves can alternately correspond to coexistence of either one or two solid phases with the aqueous solution, and vertices can alternately correspond to coexistence of either two or three solid phases in equilibrium with the solution. The 2D regions forming the surface of the figure define the range of solution compositions for which a single solid phase is in stable equilibrium with the aqueous solution. The 1D boundaries separating these phase stability surfaces define the set of compositions for which two solid phases coexist in equilibrium with the solution, and the vertices at which these boundaries meet are points at which two or three solid phases coexist in equilibrium with the solution.

Figure 1 is similar in most respects to prior constructions for this system,[8,12,45] except that Fig. 1 has a narrow AFm region that separates the stability surfaces for AFt (labeled ettringite in the figure) and hydrogarnet. This AFm phase also is a nonideal solid solution of monosulfate and C_4AH_{13}, shown in Table III. Its composition is weighted heavily toward the monosulfate end-member along all the four boundaries of its stability surface. More specifically, on a mass basis AFm contains 2.2% C_4AH_{13} at its triple point with ettringite and gibbsite, 7.4% at its triple point with hydrogarnet and gibbsite, 10.1% at its triple point with ettringite and portlandite, and 21.2% at its triple point with portlandite and hydrogarnet. The existence and compositions of these solid solution phases are based on the thermodynamic data and solid solution models described in the work of Matschei et al.[16] A more recent review article[35] shows stable coexistence of ettringite and hydrogarnet along a two-phase boundary curve at 25°C (see Fig. 3 in Ref. [36]). In contrast, Fig. 8 of the same article[36] shows that the stable regions of monosulfate and several OH–AFm phases appear

Table II. Solid Phase Compositions and Solubility Products in the Cemdata07 Supplement [16] to the Nagra-PSI Database

Name	Reaction	$\log_{10} K_{sp}$
Gibbsite	$Al(OH)_3(s) + 3H^+ \rightleftharpoons Al^{3+} + 3H_2O$	7.76
AFm-phases		
C_2AH_8	$2CaO \cdot Al_2O_3 \cdot 8H_2O(s) \rightleftharpoons 2Ca^{2+} + 2Al(OH)_4^- + 2OH^- + 3H_2O$	-13.56
C_2FH_8	$2CaO \cdot Fe_2O_3 \cdot 8H_2O(s) \rightleftharpoons 2Ca^{2+} + 2Fe(OH)_4^- + 2OH^- + 3H_2O$	-17.88
C_4AH_{13}	$4CaO \cdot Al_2O_3 \cdot 13H_2O(s) \rightleftharpoons 4Ca^{2+} + 2Al(OH)_4^- + 6OH^- + 6H_2O$	-25.40
C_4FH_{13}	$4CaO \cdot Fe_2O_3 \cdot 13H_2O(s) \rightleftharpoons 4Ca^{2+} + 2Fe(OH)_4^- + 6OH^- + 6H_2O$	-29.88
Monosulfate	$3CaO \cdot Al_2O_3 \cdot CaSO_4 \cdot 12H_2O(s) \rightleftharpoons 4Ca^{2+} + 2Al(OH)_4^- + SO_4^{2-} + 4OH^- + 6H_2O$	-29.26
AFt-phases		
Ettringite	$Ca_6Al_2(SO_4)_3(OH)_{12}(H_2O)_{26}(s) \rightleftharpoons 6Ca^{2+} + 2Al(OH)_4^- + 3SO_4^{2-} + 4OH^- + 26H_2O$	-44.9
Fe-ettringite	$Ca_6Fe_2(SO_4)_3(OH)_{12}(H_2O)_{26}(s) \rightleftharpoons 6Ca^{2+} + 2Fe(OH)_4^- + 3SO_4^{2-} + 4OH^- + 26H_2O$	-44.01
Tricarbonaluminate	$Ca_6Al_2(CO_3)_3(OH)_{12}(H_2O)_{26}(s) \rightleftharpoons 6Ca^{2+} + 2Al(OH)_4^- + 3CO_3^{2-} + 4OH^- + 26H_2O$	-41.3
Hydrogarnets		
C_3AH_6	$3CaO \cdot Al_2O_3 \cdot 6H_2O(s) \rightleftharpoons 3Ca^{2+} + 2Al(OH)_4^- + 4OH^-$	-20.84
C_3FH_6	$3CaO \cdot Fe_2O_3 \cdot 6H_2O(s) \rightleftharpoons 3Ca^{2+} + 2Fe(OH)_4^- + 4OH^-$	-26.78
CAH_{10}	$CaO \cdot Al_2O_3 \cdot 10H_2O(s) \rightleftharpoons Ca^{2+} + 2Al(OH)_4^- + 6H_2O$	-7.49
Portlandite	$Ca(OH)_2(s) + 2H^+ \rightleftharpoons Ca^{2+} + 2H_2O$	-22.80
Anhydrite	$CaSO_4(s) \rightleftharpoons Ca^{2+} + SO_4^{2-}$	-4.34
Gypsum	$CaSO_4 \cdot 2H_2O(s) \rightleftharpoons Ca^{2+} + SO_4^{2-} + 2H_2O$	-4.43
Syngenite	$K_2Ca(SO_4)_2 \cdot H_2O(s) \rightleftharpoons Ca^{2+} + 2K^+ + 2SO_4^{2-} + H_2O$	-7.2

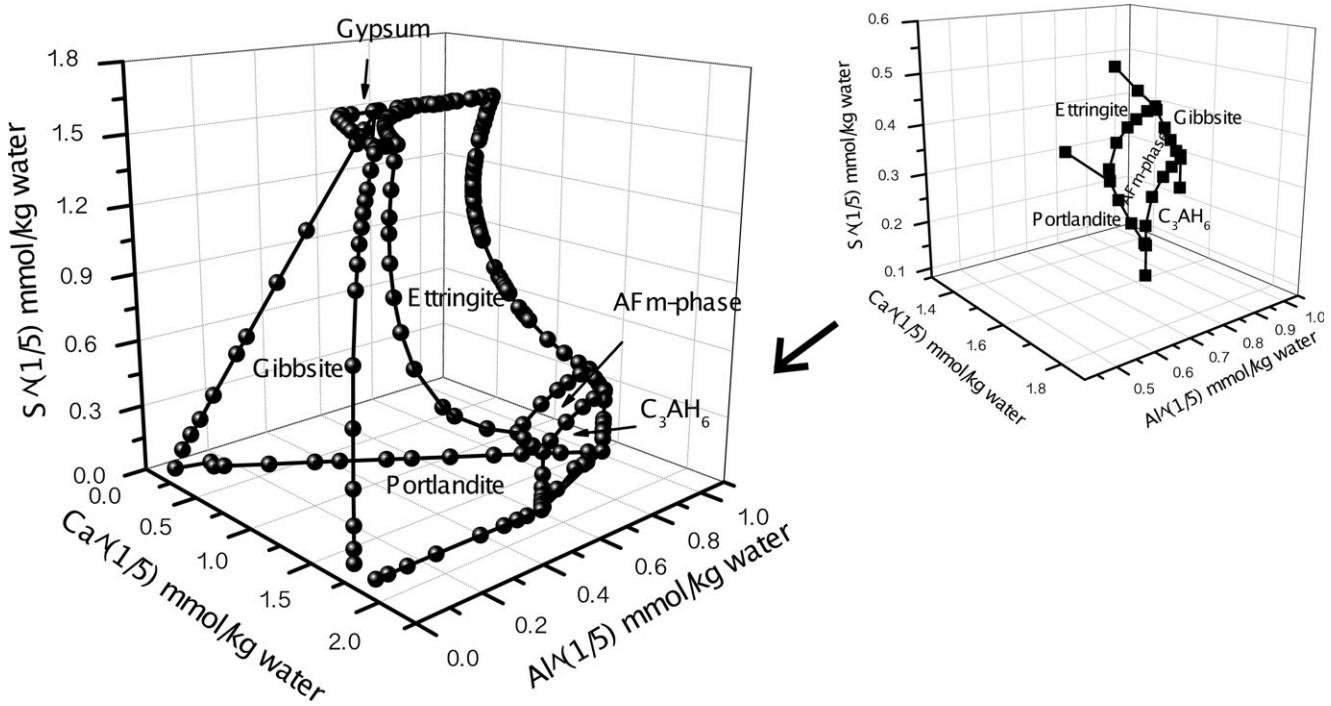

Fig. 1. Phase diagram for the Ca–Al–S–O–H system.

Table III. Solid Solution Model of AFm and AFt Phases as Implemented in the Cemdata07 Supplement[16] to the Nagra-PSI Database

Phases	End members	Composition
Monosulfate	Monosulfate	$3CaO{\cdot}Al_2O_3{\cdot}CaSO_4{\cdot}12H_2O$
	Fe-monosulfate	$3CaO{\cdot}Fe_2O_3{\cdot}CaSO_4{\cdot}12H_2O$
OH_SO4_AFm†	C_4AH_{13}	$4CaO{\cdot}Al_2O_3{\cdot}13H_2O$
	Monosulfate	$3CaO{\cdot}Al_2O_3{\cdot}CaSO_4{\cdot}12H_2O$
C_2AFH_8‡	C_2AH_8	$2CaO{\cdot}Al_2O_3{\cdot}8H_2O$
	C_2FH_8	$2CaO{\cdot}Fe_2O_3{\cdot}8H_2O$
Ettringite	Ettringite	$Ca_6Al_2(SO_4)_3(OH)_{12}(H_2O)_{26}$
	Fe-ettringite	$Ca_6Fe_2(SO_4)_3(OH)_{12}(H_2O)_{26}$
CO_3_ SO_4_AFt§	Ettringite	$Ca_6Al_2(SO_4)_3(OH)_{12}(H_2O)_{26}$
	Tricarboaluminate	$Ca_6Al_2(CO_3)_3(OH)_{12}(H_2O)_{26}$

†The OH–SO4–AFm solid solution has a sulfate-rich analog, SO4–OH–AFm, with the same end-members.
‡Not present in this system due to absence of iron.
§The CO3–SO4–AFt solid solution has a sulfate-rich analog, SO4–CO3–AFt, with the same end-members.

in the same part of the phase diagram only if hydrogarnet is excluded as a possible phase for kinetic reasons at the same temperature. For these reasons, we investigate the influence of hydrogarnet solubility on the predicted phase diagram in Section III(3).

Table IV shows the calculated elemental composition of the aqueous solution at vertices in Fig. 1 where two or three solid phases coexist in equilibrium with the solution, also showing those points calculated in an earlier study[12] for comparison. To facilitate that comparison, the ionic concentrations are all given in units of mmol/L of solution. [Ca], [Al], and [S] represent the sum of concentrations of all the aqueous species containing Ca, Al, or S, respectively. Most of the equilibrium compositions are similar, in absolute terms, to those calculated earlier.[12] In no instance does the elemental concentration of Ca, Al, or S differ by more than 2.9 mmol/L, although for Al and S, the relative differences between the two studies can be quite large when the concentrations are very low (e.g., the invariant point corresponding to equilibrium with ettringite, portlandite, and gypsum). The hydroxyl concentration, which is quite sensitive to speciation, shows more variation between the two studies, with the difference being typically about 5 mmol/L. This latter observation is not too surprising in light of refinements in measured thermodynamic properties that have been made and incorporated into the Nagra/PSI database since the earlier study[12] was performed.

(1) Influence of Alkali Species on AFt Stability

Besides the 240 equilibrium states calculated to construct the phase diagram in Fig. 1, approximately 1000 additional calculations were made for systems also spiked with Na or K at concentrations of (20, 200, or 500) mmol/kg. These calculations do not consider incorporation of alkali cations or hydroxyl anions as dissolved impurities within any solid phase, which could occur by ion exchange or surface adsorption, because the necessary solid solution models or sorption isotherms are not available for these phases. Figure 2 shows the influence of [Na] on the AFt stability surface. The topology of the phase diagram remains unchanged with increasing concentrations. That is, no new stable phases are predicted, so the AFt stability region is still defined by its boundary with the surfaces of monosulfate, gypsum, gibbsite, and port-

Table IV. Composition of the Solution at Multiphase Equilibrium Points in the Ca–Al–S–O–H System at 25°C, Comparing to Results Reported in Ref. [12]. All Concentrations Reported in Millimolar Concentration Units (mmol/L) for Equivalent Comparison Between the Two Studies

Solids in equilibrium	[Ca]	[Al]	[S]	[OH]	pH
C_3AH_6–AH_3†	8.251	1.087	0	14.442	12.097
C_3AH_6–AH_3‡	5.35	0.357	0	10.340	11.960
C_3AH_6–CH†	20.304	0.087	0	36.210	12.472
C_3AH_6–CH‡	20.96	0.007	0	41.89	12.520
Gypsum-CH†	32.129	0	12.778	33.790	12.429
Gypsum-CH‡	31.15	0	11.48	39.340	12.470
AH_3-Ettr-AFm†	6.839	0.906	0.105	12.040	12.022
AH_3–C_3AH_6–AFm†	8.253	1.087	0.002	14.441	12.097
AH_3-Ettr-Gypsum†	16.177	0.019	16.029	0.255	10.325
AH_3-Ettr-Gypsum†	15.17	0.001	15	0.340	10.430
Ettr-CH-Gypsum†	32.129	6×10^{-7}	12.778	33.790	12.429
Ettr-CH-Gypsum‡	31.3	0.0003	11.4	39.790	12.470
CH–AFm–C_3AH_6†	20.305	0.087	0.001	36.210	12.472
CH-AFm-Ettr†	20.291	0.038	0.009	36.220	12.472

†This study.
‡Reported in Ref. [12].

landite. However, with increasing [Na] the AFt surface undergoes significant translations toward lower [Ca] and higher [Al] and [S], as well as small shape changes. The 3D images are projected onto the Al–Ca plane [Fig. 2(a)] and the S–Ca plane [Fig. 2(b)], from which these trends can be perceived more easily. The same trends also were observed in Ref. [11] in which the stability boundaries were estimated by interpolating line segments through pairs of vertices rather than by calculating equilibrium states at multiple compositions between them.

Very high sodium concentrations have been reported to promote the formation of a sodium-substituted AFm phase, called the "U phase".[46] This phase has been observed in cement-based systems[47] and synthesized in the laboratory,[46] but its thermodynamic properties remain poorly characterized and it is not included in the cemdata07 database. Furthermore, the extended Debye–Hückel model, Eq. (3), for molal activity coefficients of dissolved species is known to be less accurate at these higher ionic strengths. Therefore, the calculations of AFt (and AFm) stability at the highest alkali concentrations are more speculative and should be thoroughly tested by experiment. Such experiments potentially could have the added benefits of detecting solubility limits of alkali components in the hydrate phases and of furnishing thermodynamic properties of the U phase that could be incorporated into thermodynamic databases.

The influence of potassium additions on the equilibrium surface of AFt is quite similar to that of sodium additions, as can be seen by comparing Fig. 2 for sodium with Fig. 3 for potassium. Figure 4 shows the equilibrium surfaces of AFt in both cases almost overlap with each other with only slight differences at low (20 mmol/kg) or moderate (200 mmol/kg) alkali content.

Syngenite becomes stable at the highest potassium concentration studied here, 500 mmol/kg, when [Ca], [Al], and [S] are also high. The stabilization of syngenite, reported previously by Bellmann,[48] introduces new boundary segments to the ettringite equilibrium surface, as shown in Fig. 5. Similar to its counterpart at lower [K], the ettringite surface is bounded by portlandite, monosulfate, and gibbsite when [S] in the solution is low. At higher [S], ettringite can be simultaneously in equilibrium with both gibbsite and syngenite, with both gypsum and syngenite, or with both portlandite and syngenite, along three new boundary curves—the addition of potassium to the system enabling an additional solid phase to coexist along boundary curves by Gibbs' phase rule. The new boundary curves intersect at four-phase vertices. These differ modestly from those reported in Ref. [13] in which the equilibrium surface of syngenite at high sulfate concentrations are bounded by gypsum, ettringite, and gibbsite but not portlandite. This difference is likely due to differences in the underlying thermodynamic data used in the two studies; the Gibbs energies of dissociation used in this study are based on improved solubility measurements that have been made in the intervening years.[16,19,49] Another contribution to the departure of the current syngenite stability region from that found earlier is that the method used here does not permit the setting of individual aqueous ion concentrations in solution. Instead, the calculations performed here come closer to experimental reality by permitting only the total quantity of each element to be specified by the user, even for elements, like potassium, which will have one dominant aqueous component (K^+). Thus, as described earlier, the current calculations consider a wider range of aqueous species, the concentrations of which are determined solely by minimization of the global Gibbs energy. However, the prediction of syngenite agrees with the more recent study reported by Bellmann et al.[48] in terms of the sulfate concentration at which syngenite is in equilibrium with the solution. In our calculations, the lowest sulfate concentration at which syngenite appears is 188.415 mmol/kg, close to Bellmann's value[d] of 190.625 mmol/L at pH 12.92 and 12.98, respectively.[48]

The equilibria of ettringite with other solid phases in the presence of potassium can be categorized in terms of three ranges of sulfate concentration,

1. $(1.23 \leq [S] < 13.5)$ mmol/kg: ettringite, AFm, and $Ca(OH)_2$
2. $(13.5 \leq [S] < 101.58)$ mmol/kg: ettringite, $Ca(OH)_2$, and $Al(OH)_3$
3. $(101.58 \leq [S] < 142.24)$ mmol/kg: ettringite, $Ca(OH)_2$, $Al(OH)_3$, syngenite, and gypsum

(2) Influence of Alkali Ions on AFm Phase Stability

Figure 6 shows the influence of adding Na or K on the equilibrium surface of AFm solid solution. As described in the previous section, the alkali cation's effect is primarily to modify the ionic strength and, consequently, the activities of each aqueous solution component. Therefore, both monovalent alkali cations have almost the same effect on shifting the AFm stability surface toward lower calcium and higher sul-

[d]Concentrations in Ref. [45] were given in units of mg/L, which we converted to mmol/L units by using 96 g/mol for the molar mass of SO_4^{2-}.

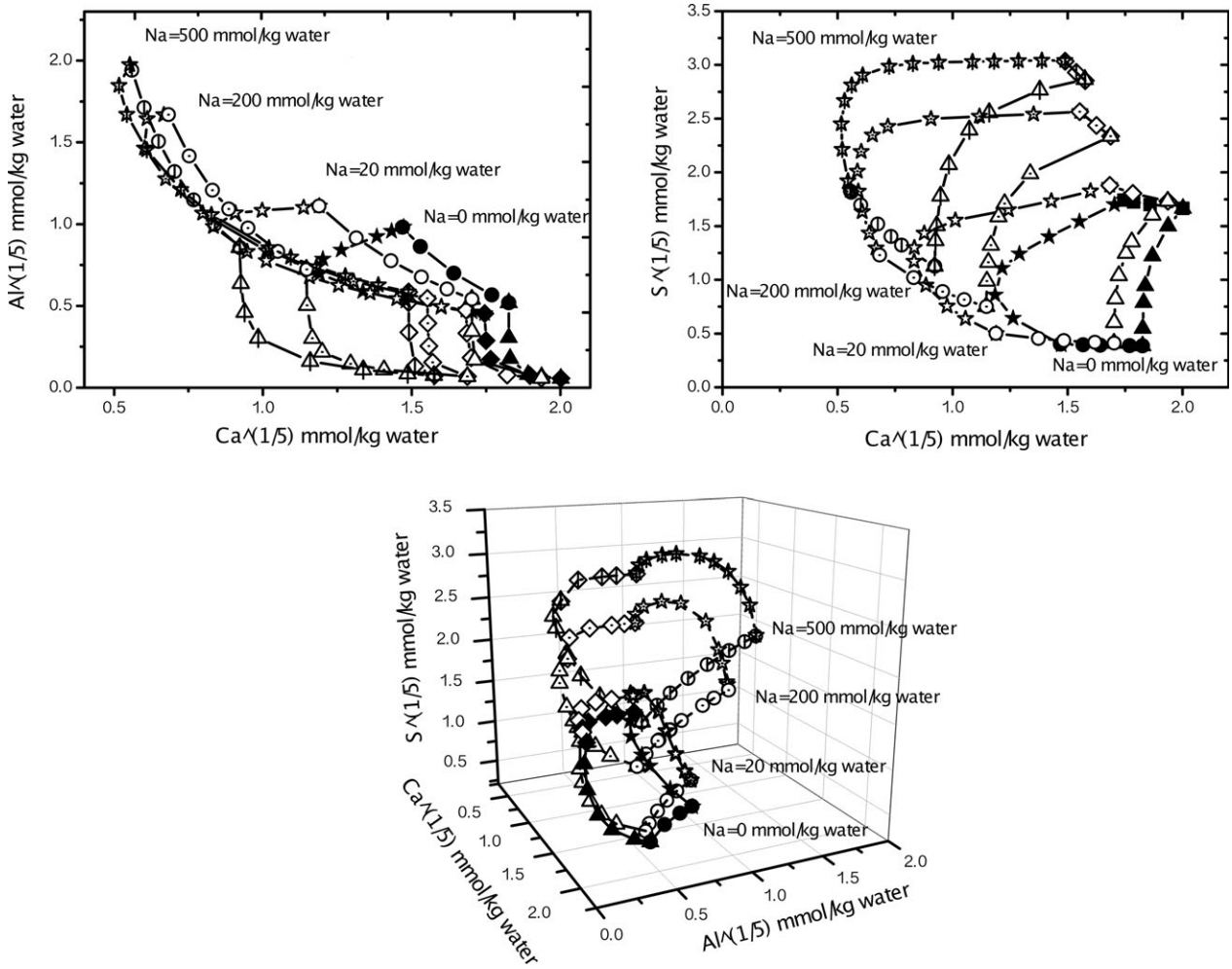

Fig. 2. The influence of Na on stability of AFt. Shift of AFt equilibrium surface on Al–Ca plane (upper left); shift of AFt equilibrium surface on S–Ca plane (upper right); 3D representation of AFt surface displacements (bottom), in which triangles represent the boundary between AFt and portlandite, squares represent the boundary between AFt and gypsum, stars represent the boundary between AFt and gibbsite, and circles represent the boundary between AFt and sulfate-rich AFm.

fate concentrations. For the four concentrations of alkali investigated in the study, the equilibrium surface of AFm is always bounded by AFt, gibbsite, hydrogarnet, and portlandite. More interestingly, the size of the AFm surface in the ([Ca]–[Al]–[S]) subspace increases significantly with increasing alkali concentration. That is, AFm should have a greater compositional range of stability as pH increases. External sulfate attack of portland cement involves the ingress of a (usually) lower pH sulfate solution that partially displaces the higher pH solution in the pores. Perhaps the most prominent contribution to sulfate attack is the transformation to AFt phases, such as ettringite, of AFm phases like monosulfate,[4,5,10,11,50] which generates crystallization pressures in the interior pores and drives expansion of the material. The calculations made here imply that the transformation of sulfate-rich AFm to AFt can be favored both by an increase in sulfate concentration and by a simultaneous reduction in pH. A general trend, though not directly evident in Fig. 6, is that increasing alkali concentration modestly reduces the proportion of the C_4AH_{13} endmember of the AFm solid solution.

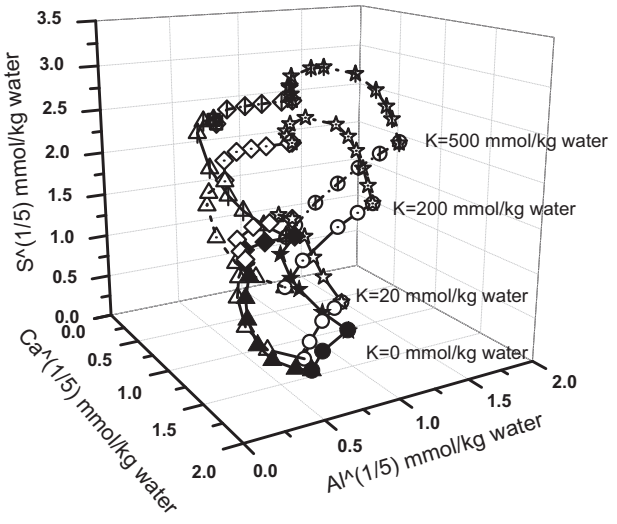

Fig. 3. The influence of K on stability of AFt.

(3) Influence of Hydrogarnet Solubility

Figure 1 indicates that the stable region predicted for AFm is bounded by hydrogarnet and ettringite at lower and higher sulfur concentrations, respectively. The size of the stable AFm phase region is therefore dependent on the solubility of hydrogarnet and of ettringite. Reported values of $\log_{10}K_{sp}$ for ettringite, when expressed using the same dissolution reaction, vary within a narrow range very near the value of −44.9 used in the cemdata07 database.[16,51] However,

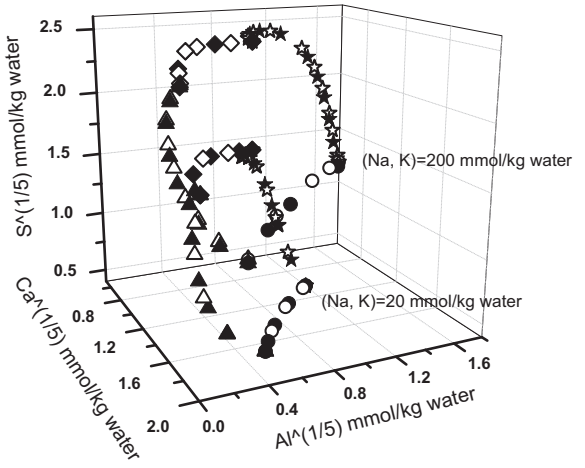

Fig. 4. Comparison of the influences of K and Na on the stability of AFt.

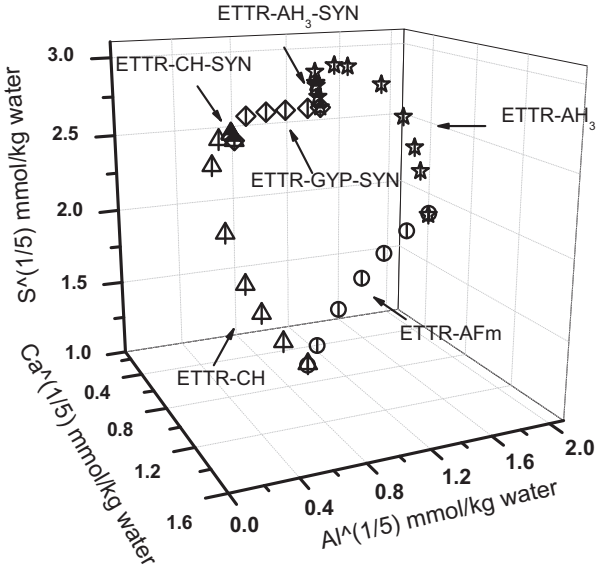

Fig. 5. Equilibrium surface of AFt when [K] = 500 mmol/kg.

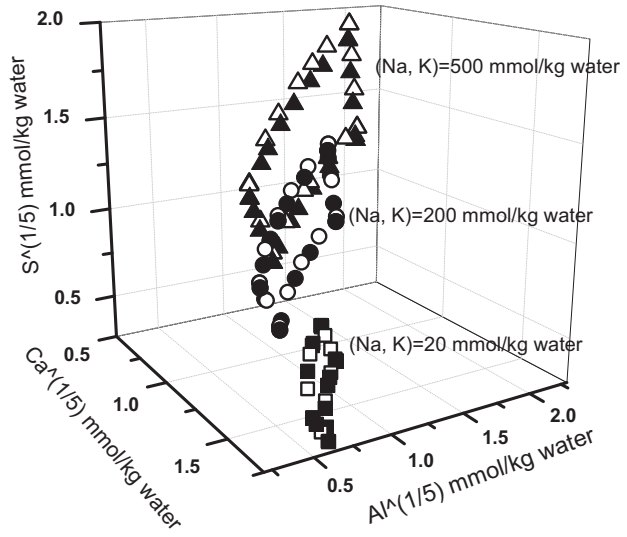

Fig. 6. Influence of alkali ions on the stability of sulfate-rich AFm solid solution. The boundaries of the equilibrium surface are represented by solid symbols when Na is added, and by open symbols when K is added.

reported values for hydrogarnet's solubility product, corresponding to the dissociation reaction

$$3CaO \cdot Al_2O_3 \cdot 6H_2O \leftrightarrows 3Ca^{2+} + 2AlO_2^- + 4OH^- + 4H_2O \quad (6)$$

vary by more than two orders of magnitude, as shown in Table V, with the value used in this study lying between the extremes.

One can check the sensitivity to hydrogarnet solubility of AFm phase stability region by varying hydrogarnet's assumed solubility product in the thermodynamic database, for example, in the range $-22.46 \le \log_{10} K_{sp} \le -19.5$ as indicated in Table V. This is accomplished within the GEM model by assigning different values for the standard Gibbs energy for reaction (6) at 298 K according to $\Delta G^\circ \equiv -RT \ln K_{sp}$, where R is the ideal gas constant and T is the absolute temperature. Figure 7 shows how the position and size of the AFm stability region depends on K_{sp} for hydrogarnet. In particular, its boundary contracts—and that of hydrogarnet expands—monotonically with decreasing hydrogarnet K_{sp}. This happens exclusively by an upward shift in the boundary between hydrogarnet and AFm toward higher sulfur concentrations. As expected, the range of aluminum concentrations over which AFm is stable remains about the same because it depends only on the relative stability of AFm with respect to portlandite and gibbsite, not hydrogarnet. For the same reason, the phase boundary between AFm phase and ettringite, that is, the upper bound of sulfate concentration for AFm, also remains essentially fixed.

When $\log_{10} K_{sp}$ of hydrogarnet reaches the highest (i.e., most soluble) value used in our calculations, a new but narrow region appears on the AFm solid solution surface that extends down to low sulfate concentrations. This new region separates the hydrogarnet and portlandite regions; hydrogarnet with this high solubility cannot exist in equilibrium with portlandite. The new region of the AFm surface corresponds to a spinodal decomposition by which the homogeneous AFm solid solution, with monosulfate and C_4AH_{13} end-members, separates into two solid solutions, both having those same two end-members, but with one being considerably enriched in C_4AH_{13} (97% C_4AH_{13} by mass). As expected, this miscibility gap for the AFm phase is consistent with solubility data reported in Fig. 4 of Ref. [17] occurring when $SO_4/(SO_4 + OH) = 0.5$.

Table VI lists the compositions of AFm solid solutions as a function of solubility of hydrogarnet. One can observe the significant increase in C_4AH_{13} within AFm as hydrogarnet becomes more soluble. Similar results are reported by Damidot et al.,[36] in which C_4AH_{13} as well as other OH–AFm phases are predicted to become stable if hydrogarnet is excluded from consideration on the basis that it is not usually observed in early hydration products[36] and is rarely detected in cement paste at room temperature.[16] In this case, C_4AH_{13} should precipitate along with other OH-AFm phases as suggested by Fig. 7.

The AFm solid solution phase is unstable if $\log_{10} K_{sp} \le -21.53$ for hydrogarnet because AFm–hydrogarnet phase boundary coincides with the upper AFm–ettringite boundary, replacing the AFm surface with a new phase boundary between ettringite and hydrogarnet. At this point of instability, the new ettringite-hydrogarnet phase boundary is located exactly where the previous AFm–ettringite phase boundary had been. Further decreases in hydrogarnet solubility cause this phase boundary to be pushed to higher sulfur concentrations where formerly ettringite had been the only stable phase.

The calculated sensitivity of the stability of AFm on the solubility of hydrogarnet underscores the importance of accurate experimental data on the Gibbs energy of dissociation for hydrogarnet and other solid phases. Nevertheless, as

Table V. Hydrogarnet Solubility Products Reported in the Literature and Used in This Study

$\log_{10} K_{sp}$	Reference
−19.95	Reardon[57]
−20.84	GEMIPM3K database (this study)
−21.20	Sinitsyn et al.[58]
−20.29–22.24	Matschei et al.[16]
−21.42	Blanc et al.[47]
−22.30	Nikuschenko et al.[59]
−22.46	Berner and Kulik[19,46]

shown here, thermodynamic calculations can provide insight about how these complex equilibria are quantitatively influenced by the uncertainty in such data, and can even furnish estimates of the maximum uncertainty that can be tolerated without qualitatively influencing the phase diagram.

(4) Influence of Carbonate on the pH Sensitivity of AFm and AFt

The addition of fine limestone to cement is increasingly common as it reduces the carbon footprint of cement.[36] Just as importantly, cementitious binders encounter carbonates by prolonged exposure to air, in which CO_2 is typically present at concentrations of about 400 parts per million (ppm). Therefore, depending on depth below the air surface, hydrated cement binders may incorporate a broad range of carbonate concentrations even if limestone is not added intentionally. Previous experimental observations and thermodynamic calculations have indicated that carbonates can prevent the transformation of AFt to sulfate-rich AFm during hydration, during which time the pH of the pore solution typically exceeds 13, by stabilizing calcium monocarboaluminate hydrate.[2,35,52–55] However, we found no information in the literature about how carbonates influence phase stability in lower pH pore solutions that are encountered in several forms of concrete degradation, such as leaching, sulfate attack, and carbonation itself. We now investigate this further by adding a carbonate source to the system and intentionally varying the pH with alkali additions.

Four systems were simulated, all having the same content of $Al(OH)_3$ (60 mmol/kg), $Ca(OH)_2$ (150 mmol/kg), and $CaSO_4$ (45 mmol/kg) but with $CaCO_3$ content of (0, 6, 10, or 18) mmol/kg. The solution pH in each system was adjusted by adding anywhere between 0 mmol/kg and 0.78 mmol/kg of Na_2O to vary the pH from around 12 to 14, the typical range for pore solution of portland cement. The increased number of system components means that up to four solid phases can coexist with aqueous solution at equilibrium, so phase relations are more difficult to visualize with a 3D phase diagram. Therefore, we plot instead the solid phase mass contents as a function only of pH in Fig. 8. The figure demonstrates not only the well-known fact that the amount of portlandite decreases steadily with decreasing pH—the basis of leaching phenomena—but also that the carbonate content has a significant influence on the pH ranges in which different AFm-type phases are stable. The phase assemblages shown in this figure generally agree with Fig. 1 in Ref. [56] when plotted in terms of CO_2/Al_2O_3 and SO_3/Al_2O_3 ratios. Calcite, which is normally observed to persist when added to cement paste, is not present in Fig. 8 because the maximum concentration of carbonates added is too low to achieve saturation with respect to calcite.

Figure 8 shows that monocarbonate (that is, calcium monocarboaluminate hydrate) is the only stable AFm phase throughout the pH range studied, if sufficient carbonate is available for its formation [see Fig. 8(d)]. At lower carbonate concentrations [Figs. 8(b) and (c)], monocarbonate content is diminished in favor of SO_4–OH–AFm, for pH > 13.5, or calcium hemicarboaluminate hydrate for pH < 13.5. The influence of carbonate addition on decreasing SO_4–OH–AFm in favor of carbonate-based AFm is more significant at lower pH.

Although not shown explicitly in the figure, higher carbonate additions cause a small concentration of carbonate to be dissolved in the AFt solid solution. Beyond the increased carbonate content in AFt, Figure 8 also shows that the mass fraction of AFt increases considerably with the addition of carbonates to the system, especially at lower pH. This observation is consistent with previous reports.[2,36,52,53]

Taken together with Section III(1), these results provide additional clarity on the beneficial effects that have been reported on limestone additions to portland cement for enhancing sulfate resistance.[50] High alkali environments tend to stabilize monosulfate-based AFm relative to ettringite. Infiltration of hydrated cement by a low pH sulfate solution promotes the expansive conversion of sulfate-rich AFm to AFt because of both the higher sulfate availability and the lower pH environment. Addition of a soluble carbonate to portland cement favors both AFt and carbonate-based AFm over sulfate-based AFm, particularly in the low pH conditions caused by infiltration of sulfate solutions, and therefore reduces or eliminates the transformation of sulfate-rich AFm to AFt. Figure 8 suggests that greater carbonate additions would be required to promote the same degree of sulfate

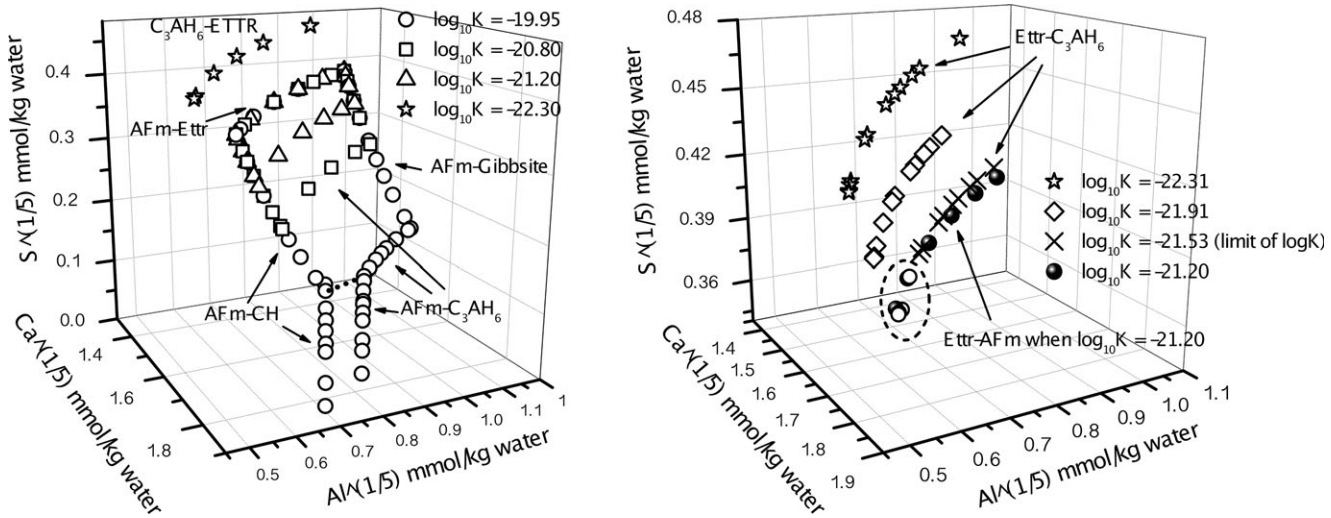

Fig. 7. Influence of assumed hydrogarnet solubility product on stability surface of AFm. The circled region on the right plot shows the appearance of sulfate-rich AFm when $\log_{10} K = -21.53$.

Table VI. Compositions of AFm Solid Solutions as a Function of Solubility of Hydrogarnet. The Compositions of the Solid Solution are Expressed in Mass Percentage of Each End-Member. The Label "spinodal" Refers to the Stability Limit Marked by the Dashed Line in Fig. 7

Hydrogarnet $\log_{10} K_{sp}$	Boundary	C_4AH_{13} (%)	Monosulfate (%)
−19.95	AFm-Ettringite-Portlandite	10.1	89.9
−19.95	AFm-Ettringite-Gibbsite	2.2	97.8
−19.95	AFm-Gibbsite-C_3AH_6	25.8	74.2
−19.95	AFm-C_3AH_6-spinodal	49.6	50.4
−19.95	AFm-Portlandite-spinodal	47.7	52.3
−21.20	AFm-Ettringite-Portlandite	10.1	89.9
−21.20	AFm-Ettringite-Gibbsite	2.2	97.8
−21.20	AFm-Gibbsite-C_3AH_6	3.9	96.1
−21.20	AFm-C_3AH_6-portlandite	14.8	85.2

resistance at high pH. Typical limestone additions to portland cement, often 5% or more by mass, are more than sufficient to provide sulfate resistance even under the highest pH conditions examined here. However, as reported elsewhere,[50,60] there is an upper limit to the limestone addition levels beyond which its dilution of the hydraulic components leads to higher capillary porosity during hydration and, consequently, greater susceptibility to deterioration by ingress of external solutions. Furthermore, the presence of limestone in concretes with excess sulfates raises the possibility of thaumasite formation.[50] Thaumasite formation is extremely deleterious to concrete properties, but the current calculations at 25°C do not consider thaumasite because it is usually not observed to form in significant amounts at temperatures exceeding 8°C, even when sufficient carbonates and sulfates are present.[50]

IV. Conclusion

GEM at constant temperature, pressure, and elemental composition, using an expanded and improved thermodynamic database for cementitious materials, has been used to revisit the predicted equilibria in the Ca–Al–S–O–H system. The new calculations take advantage of more comprehensive and accurate thermodynamic properties of solid cementitious phases and of ion complexes in solution that have been measured in recent years and made available through public databases.[16,19,35] We have focused on how the stabilities of AFm and AFt phases in the Ca–Al–S–O–H system depend on the presence of alkali or carbonate additions, because these factors are present in portland cement binder materials and because their effects on these phases has not received as much detailed attention in the modeling literature.

Not surprisingly, the size and shape of the stability region of sulfate-rich AFm is determined not only by the solubility products of its end-members, but also by the solubility products of adjacent solid phases in the phase diagram. The measured or assumed solubility product of hydrogarnet, in particular, has varied considerably in the literature, and the use of lower hydrogarnet solubility is the likely reason that monosulfate-based AFm is sometimes taken to be unstable.

Sodium and potassium additions can significantly increase the composition range over which sulfate-rich AFm is stable relative to AFt. Either Na or K shifts the equilibrium

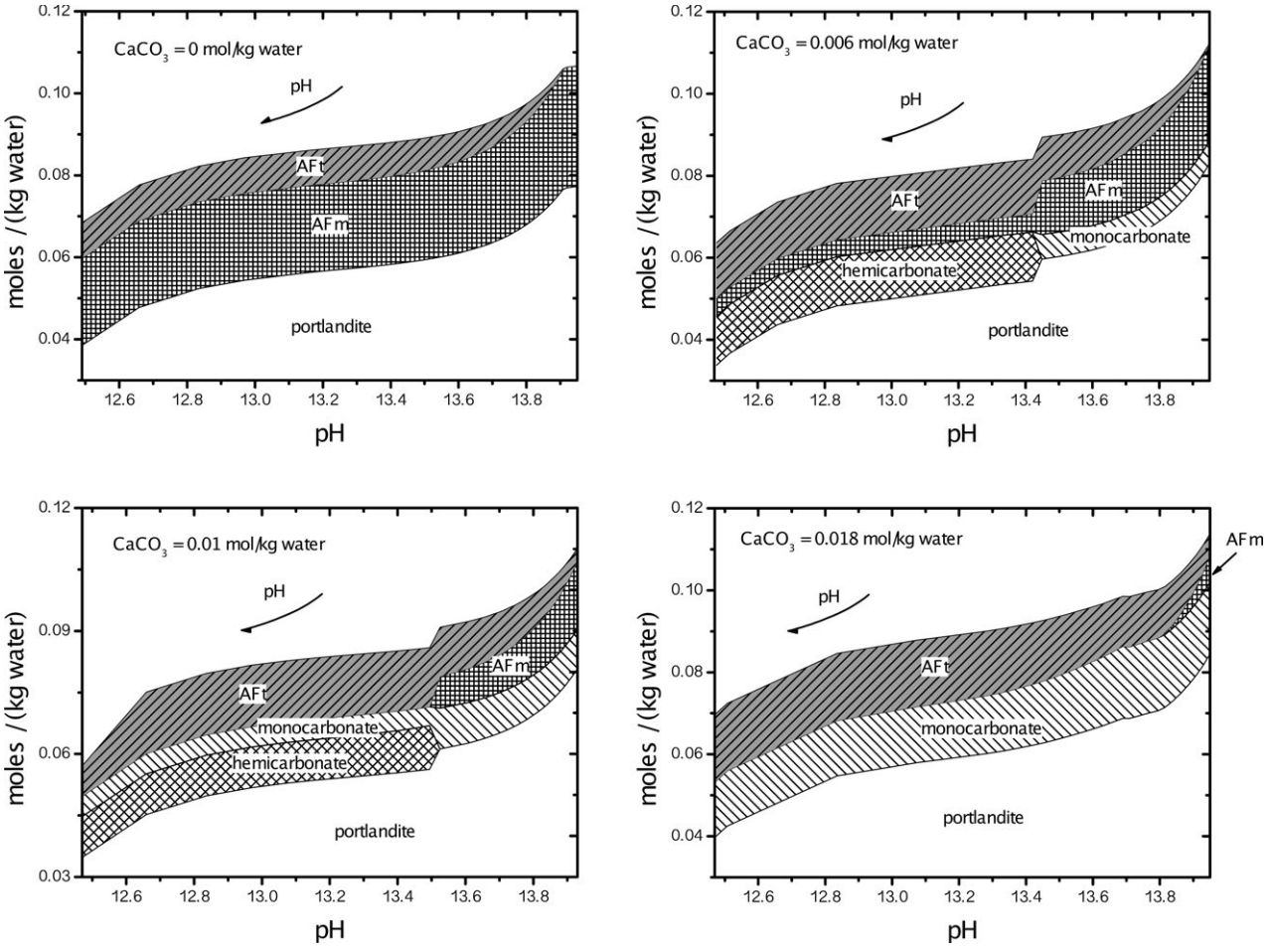

Fig. 8. Influence of carbonate additions on the pH sensitivity of AFm and AFt.

between AFt and AFm to higher sulfate and aluminate concentrations and to lower calcium concentrations. The stability region of sulfate-rich AFm is thereby enlarged as pH increases. Therefore, the expansive transformation from monosulfate to ettringite that characterizes external sulfate attack is exacerbated by ingress of sulfate solutions that displace alkali ions and lower the pH.

$CaCO_3$, which at low addition levels is known to increase the sulfate resistance of portland cement binders, has a large influence on the stability and pH sensitivity of AFm phases. Even small carbonate additions push the stability of sulfate-rich AFm to higher pH while favoring hemicarbonate or monocarbonate AFm phases at lower pH. And sufficiently high carbonate dosages (e.g., $CO_3/SO_4 > 0.4$) effectively destabilize sulfate-rich AFm in favor of monocarbonate over the entire pH range relevant to portland cement systems.

These conclusions are based solely on GEM using the most accurate and comprehensive thermodynamic property database for cementitious mineral phases of which we are aware. However, the calculations involve several assumptions and so should be independently tested by experimental measurements, especially where those assumptions might be questionable. In particular, the predicted influence on AFm and AFt stability of alkali components at high concentrations, exceeding 200 mmol/kg, should be tested because of the possibility of alkali incorporation as dissolved solid solution components and the possible formation at high sodium concentrations of the U phase, both of which have been neglected here due to lack of the required solubility data. In addition, the pH-dependent stability limit of SO_4-rich AFm at low carbonate concentrations deserves further experimental scrutiny, especially because of its relevance to positively affecting the sulfate resistance of cementitious binders, even in the absence of intentionally added limestone.

Acknowledgment

All research reported in this article was performed at the National Institute of Standards and Technology (NIST). Pan Feng gratefully acknowledges financial support from the Chinese Scholarship Council and from the NIST Engineering Laboratory. Ken Snyder and an anonymous reviewer are both warmly thanked for providing valuable reviews that greatly improved the manuscript.

References

[1]G. Le Saout, B. Lothenbach, A. Hori, T. Higuchi, and F. Winnefeld, "Hydration of Portland Cement with Additions of Calcium Sulfoaluminates," *Cem. Concr. Res.*, **43**, 81–94 (2013).

[2]B. Lothenbach, G. Le Saout, E. Gallucci, and K. Scrivener, "Influence of Limestone on the Hydration of Portland Cements," *Cem. Concr. Res.*, **38**, 848–60 (2008).

[3]P. W. Brown and H. F. W. Taylor. "The Role of Ettringite in External Sulfate Attack"; pp. 73–98 in *Materials Science of Concrete: Sulfate Attack Mechanisms*, Edited by J. Marchand and J. P. Skalny. American Ceramic Society, Westerville, Ohio, 1999.

[4]J. R. Clifton and J. M. Pommersheim, "Sulfate Attack of Cementitious Materials: Volumetric Relations and Expansions"; NIST Interagency Report 5390, National Institute of Standards and Technology, Gaithersburg, Maryland, April 1994.

[5]R. S. Gollop and H. F. W. Taylor, "Microstructural and Microanalytical Studies of Sulfate Attack I. Ordinary Portland Cement Paste," *Cem. Concr. Res.*, **22**, 1027–38 (1992).

[6]I. Baur, D. Keller, B. Wehrli, and A. Johnson, "Dissolution-Precipitation Behaviour of Ettringite, Monosulfate, and Calcium Silicate Hydrate," *Cem. Concr. Res.*, **34**, 341–8 (2004).

[7]G. L. Kalousek, "Sulfoaluminates of Calcium as Stable and Metastable Phases, and a Study of a Portion of the Five-Component System $CaO–SO_3–Al_2O_3–Na_2O–H_2O$ at 25°C"; Ph.D. Thesis, University of Maryland, College Park, MD, 1941.

[8]F. E. Jones, "The Quaternary System $CaO–Al_2O_3–CaSO_4–H_2O$ at 25°C; Equilibria with Crystalline $Al_2O_3·3H_2O$, Alumina gel and Solid Solutions," *J. Phys. Chem.*, **48**, 311–50 (1944).

[9]A. Gabrisová, J. Havlica, and S. Sahu, "Stability of Calcium Sulphoaluminate Hydrates in Water Solutions with Various pH Values," *Cem. Concr. Res.*, **21**, 1023–7 (1991).

[10]P. W. Brown and J. V. Bothe Jr, "The Stability of Ettringite," *Cem. Concr. Res.*, **5**, 47–63 (1993).

[11]D. Damidot, M. Atkins, A. Kindness, and F. P. Glasser, "Sulphate Attack on Concrete: Limits of the AFt Stability Domain," *Cem. Concr. Res.*, **22**, 229–34 (1992).

[12]D. Damidot and F. P. Glasser, "Thermodynamic Investigation of the $CaO–Al_2O_3–CaSO_4–H_2O$ System at 25°C and the Influence of Na_2O," *Cem. Concr. Res.*, **23**, 221–38 (1993).

[13]D. Damidot and F. P. Glasser, "Thermodynamic Investigation of the $CaO–Al_2O_3–CaSO_4–K_2O–H_2O$ System at 25°C," *Cem. Concr. Res.*, **23**, 1195–204 (1993).

[14]F. P. Glasser, A. Kindness, and S. A. Stronach, "Stability and Solubility Relationships in AFm Phases. Part I. Chloride, Sulfate and Hydroxide," *Cem. Concr. Res.*, **29**, 861–6 (1999).

[15]B. Albert, B. Guy, and D. Damidot, "Water Chemical Potential: A Key Parameter to Determine the Thermodynamic Stability of Some Hydrated Cement Phases in Concrete?" *Cem. Concr. Res.*, **36**, 783–90 (2006).

[16]T. Matschei, B. Lothenbach, and F. P. Glasser, "Thermodynamic Properties of Portland Cement Hydrates in the System $CaO–Al_2O_3–SiO_2–CaSO_4–CaCO_3–H_2O$," *Cem. Concr. Res.*, **37**, 1379–410 (2007).

[17]T. Matschei, B. Lothenbach, and F. P. Glasser, "The AFm Phase in Portland Cement," *Cem. Concr. Res.*, **37**, 118–30 (2007).

[18]D. A. Kulik and M. Kersten, "Aqueous Solubility Diagrams for Cementitious Waste Stabilization Systems. II, End-Member Stoichiometries of Ideal Calcium Silicate Hydrate Solid Solutions," *J. Am. Ceram. Soc.*, **84**, 3017–26 (2001).

[19]B. Lothenbach and F. Winnefeld, "Thermodynamic Modelling of the Hydration of Portland Cement," *Cem. Concr. Res.*, **36**, 209–26 (2006).

[20]D. A. Kulik, U. Berner, and E. Curti, "Modelling Chemical Equilibrium Partitioning with the GEMS-PSI Code"; pp. 109–22 in *Nuclear Energy and Safety, Volume IV of PSI Scientific Report*, Edited by B. Smith and B. Gschwend. Paul Scherrer Institut, Villigen, Switzerland, 2004.

[21]D. A. Kulik, "GEMS-PSI 2.03"; http://les.web.psi.ch/Software/GEMS-PSI/, 2009. [Online; accessed 2015-01-20].

[22]A. H. Truesdell and B. J. Jones, "WATEQ, a Computer Program for Calculating Chemical Equilibria of Natural Waters," *J. Res. US Geol. Surv.*, **2**, 233–74 (1974).

[23]J. C. Westall, J. L. Zachary, and F. M. M. Morel, "MINEQL—A Computer Program for the Calculation of Chemical Equilibrium Compositions of Aqueous Systems"; Technical note, Massachusetts Institute of Technology Dept. of Civil Engineering, Cambridge, Massachusetts, 1976.

[24]D. L. Parkhurst and C. A. J. Appelo, "Description of Input and Examples for PHREEQC Version 3-a Computer Program for Speciation, Batch-Reaction, one Dimensional Transport, and Inverse Geochemical Calculations"; http://pubs.usgs.gov/tm/06/a43, 2013

[25]L. N. Plummer, D. L. Parkhurst, G. W. Fleming, and S. A. Dunkle, "PHRQPITZ—A Computer Program Incorporating Pitzer's Equations for Calculation of Geochemical Reactions in Brines"; Water resources investigations report, U.S. Geological Survey, Denver, Colorado, 1988.

[26]J. van der Lee, "Thermodynamic and Mathematical Concepts of CHESS"; Technical report no. lhm/rd/98/39, Ecole des mines of Paris, Fontainebleau, France, 1998.

[27]C. E. Harvie, J. P. Greenberg, and J. H. Weare, "A Chemical Equilibrium Algorithm for Highly Non-Ideal Multiphase Systems: Free Energy Minimization," *Geochim. Cosmochim. Acta*, **51**, 1045–57 (1987).

[28]B. Lothenbach, T. Matschei, G. Möschner, and F. P. Glasser, "Thermodynamic Modelling of the Effect of Temperature on the Hydration and Porosity of Portland Cement," *Cem. Concr. Res.*, **38**, 1–18 (2008).

[29]B. Lothenbach, D. Damidot, T. Matschei, and J. Marchand, "Thermodynamic Modelling: State of Knowledge and Challenges," *Adv. Cem. Res.*, **22**, 211–23 (2010).

[30]M. Rafal, J. Berthold, and D. Linz, "Introduction to OLI Electrolytes"; http://www.olisystems.com/IntroElectrolytes.pdf [Online; accessed 2015-09-08].

[31]D. L. Beau, "Action of the Carbon Dioxide and of the Calcareous Granulates on the Calcium Aluminate Hydrates at the Equilibrium. Influence of the Sulphate Ions. Reaction of the Calcium Oxide Finely Pulverized with the Sodium Silicate in Alkaline Solutions. *(in Fr.)*"; Ph.D. Thesis, University of Burgundy, Dijon, France, 1991.

[32]H. Gamsja¨ger, E. Königsberger, and W. Preis, "Lippmann Diagrams: Theory and Application to Carbonate Systems," *Aquat. Geochem.*, **6**, 119–32 (2000).

[33]P. D. Glynn, "MBSSAS: A Code for the Computation of Margules Parameters and Equilibrium Relations in Binary Solid-Solution Aqueous-Solution Systems," *Comput. Geosci.*, **17**, 907–66 (1991).

[34]H. Gamsjäger and E. Königsberger, "Solubility of Sparingly Soluble Ionic Solids in Liquids"; pp. 316–58 in *The Experimental Determination of Solubilities*, Edited by G. T. Hefter and R. P. T. Tomkins. John Wiley & Sons, Hoboken, NJ, 2003.

[35]W. Hummel, U. Berner, E. Curti, F. J. Pearson, and T. Thoenen, *Nagra/PSI Chemical Thermodynamic Data Base 01/01*. Universal Publishers, Parkland, Florida, 2002.

[36]D. Damidot, B. Lothenbach, D. Herfort, and F. P. Glasser, "Thermodynamics and Cement Science," *Cem. Concr. Res.*, **41**, 679–95 (2011).

[37]I. K. Karpov, K. V. Chudnenko, D. A. Kulik, O. V. Avchenko, and V. A. Bychinskii, "Minimization of Gibbs Free Energy in Geochemical Systems by Convex Programming," *Geochem. Int.*, **39**, 1108–19 (2001).

[38]I. K. Karpov, K. V. Chudnenko, and D. A. Kulik, "Modelling Chemical Mass Transfer in Geochemical Processes: Thermodynamic Relations, Conditions of Equilibria, and Numerical Algorithms," *Am. J. Sci.*, **297**, 767–806 (1997).

[39]H. F. W. Taylor. *Cement Chemistry*, 2nd edition. Thomas Telford, London, 1997.
[40]F. G. Buttler, L. S. D. Glasser, and H. F. W. Taylor, "Studies on 4 $CaO{\cdot}Al_2O_3{\cdot}13\ H_2O$ and the Related Natural Mineral Hydrocalumite," *J. Am. Ceram. Soc.*, **42**, 121–6 (1959).
[41]R. Allmann, "Refinement of the Hybrid Layer Structure $[Ca_2Al(OH)_6]^+[1/2SO_4{\cdot}3\ H_2O]$," *Neues Jahrb. Mineral. Monatsh.*, **1977**, 136–44 (1977).
[42]M. Francois, G. Renaudin, and O. Evrard, "A Cementitious Compound with Composition $3CaO{\cdot}Al_2O_3{\cdot}CaCO_3{\cdot}11H_2O$," *Acta Crystallogr. C*, **54**, 1214–7 (1998).
[43]G. Renaudin, M. Francois, and O. Evrard, "Order and Disorder in the Lamellar Hydrated Tetracalcium Monocarboaluminate Compound," *Cem. Concr. Res.*, **29**, 63–9 (1999).
[44]H. Poellmann, "Solid Solution in the System $3CaO{\cdot}Al_2O_3{\cdot}CaSO_4{\cdot}$aq–$3CaO{\cdot}Al_2O_3{\cdot}Ca(OH)_2{\cdot}$aq," *Neues Jahrb. Mineral. Abh.*, **161**, 27–41 (1989).
[45]F. E. Jones, "The Quaternary System $CaO–Al_2O_3–CaSO_4–H_2O$ at 25°C," *Trans. Faraday Soc.*, **35**, 1484–510 (1939).
[46]G. Li, P. Le Bescop, and M. Moranville-Regourd, "Synthesis of the U Phase (4CaO·0.9Al2O3·1.1SO3·0.5Na2O·16H2O)," *Cem. Concr. Res.*, **27**, 7–13 (1997).
[47]A. Shayan, G. W. Quick, and C. J. Lancucki, "Morphological, Mineralogical and Chemical Features of Steam-Cured Concretes Containing Densified Silica Fume and Various Alkali Levels," *Adv. Cem. Res.*, **5**, 151–62 (1993).
[48]F. Bellmann, B. Möser, and J. Stark, "Influence of Sulfate Solution Concentration on the Formation of Gypsum in Sulfate Resistance Test Specimen," *Cem. Concr. Res.*, **36**, 358–63 (2006).
[49]U. R. Berner and D. A. Kulik, "Ca–Al–Hydrates: Solid Solutions?" *Geochim. Cosmochim. Acta*, **66**(Suppl. 1), A73 (2002).
[50]T. Schmidt, B. Lothenbach, M. Romer, J. Neuenschwander, and K. Scrivener, "Physical and Microstructural Aspects of Sulfate Attack on Ordinary and Limestone Blended Portland Cements," *Cem. Concr. Res.*, **39**, 1111–21 (2009).
[51]P. Blanc, X. Bourbon, A. Lassin, and E. Gaucher, "Chemical Model for Cement-Based Materials: Thermodynamic Data Assessment for Phases Other Than CSH," *Cem. Concr. Res.*, **40**, 1360–74 (2010).
[52]V. L. Bonavetti, V. F. Rahhal, and E. F. Irassar, "Studies on the Carboaluminate Formation in Limestone Filler-Blened Cements," *Cem. Concr. Res.*, **31**, 853–9 (2001).
[53]G. Kakali, S. Tsivilis, E. Aggeli, and M. Bati, "Hydration Products of C_3A, C_3S and Portland Cement in the Presence of $CaCO_3$," *Cem. Concr. Res.*, **30**, 1073–7 (2000).
[54]T. Matschei, "Thermodynamics of Cement Hydration"; Ph.D. Thesis, University of Aberdeen, Aberdeen, UK, 2009.
[55]T. Matschei and F. P. Glasser, "Temperature Dependence, 0 to 40°C, of the Mineralogy of Portland Cement Paste in the Presence of Calcium Carbonate," *Cem. Concr. Res.*, **40**, 763–77 (2010).
[56]T. Matschei, B. Lothenbach, and F. P. Glasser, "The Role of Calcium Carbonate in Cement Hydration," *Cem. Concr. Res.*, **37**, 551–8 (2007).
[57]E. J. Reardon, "An Ion Interaction Model for the Determination of Chemical Equilibria in Cement/Water System," *Cem. Concr. Res.*, **20**, 175–92 (1990).
[58]V. A. Sinitsyn, D. A. Kulik, M. S. Khororivsky, and I. K. Karpov, "Prediction of Solid-Aqueous Equilibria in Cementitious Systems Using Gibbs Energy Minimization: I. Multiphase Aqueous Ideal Solution Models," *Mater. Res. Soc. Symp. Proc.*, **506**, 953–60 (1998).
[59]V. M. Nikushchenko, V. S. Khotimchenko, P. F. Rumyantsev, and A. I. Kalinin, "Determination of the Standard Free Energies of Formation of Calcium Hydroxyaluminates," *Cem. Concr. Res.*, **3**, 625–32 (1973).
[60]E. F. Irassar, V. I. Bonavetti, and M. Gonzalez, "Microstructural Study of Sulfate Attack on Ordinary and Limestone Portland Cements at Ambient Temperature," *Cem. Concr. Res.*, **33**, 31–41 (2003). □